doi:10.1111/mmi.13118

A coiled coil switch mediates cold sensing by the thermosensory protein DesK

Emilio Saita,[1†] Luciano A. Abriata,[2†] Yi Ting Tsai,[1] Felipe Trajtenberg,[3] Thomas Lemmin,[2] Alejandro Buschiazzo,[3,4] Matteo Dal Peraro,[2] Diego de Mendoza[1*] and Daniela Albanesi[1*]

[1]*Laboratorio de Fisiología Microbiana, Instituto de Biología Molecular y Celular de Rosario (IBR), CONICET, Facultad de Ciencias Bioquímicas y Farmacéuticas, Universidad Nacional de Rosario, Ocampo y Esmeralda, Predio CONICET Rosario, 2000, Rosario, Argentina.*

[2]*Laboratory for Biomolecular Modeling, School of Life Sciences, École Polytechnique Fédérale de Lausanne (EPFL), Swiss Institute of Bioinformatics (SIB), AAB011 Station 19, 1015, Lausanne, Switzerland.*

[3]*Institut Pasteur de Montevideo, Unit of Protein Crystallography, Mataojo 2020, Montevideo, 11400, Uruguay.*

[4]*Département de Biologie Structurale et Chimie, Institut Pasteur, 25 rue du Dr. Roux, Paris, 75015, France.*

Summary

The thermosensor histidine kinase DesK from *Bacillus subtilis* senses changes in membrane fluidity initiating an adaptive response. Structural changes in DesK have been implicated in transmembrane signaling, but direct evidence is still lacking. On the basis of structure-guided mutagenesis, we now propose a mechanism of DesK-mediated signal sensing and transduction. The data indicate that stabilization/destabilization of a 2-helix coiled coil, which connects the transmembrane sensory domain of DesK to its cytosolic catalytic region, is crucial to control its signaling state. Computational modeling and simulations reveal couplings between protein, water and membrane mechanics. We propose that membrane thickening is the main driving force for signal sensing and that it acts by inducing helix stretching and rotation prompting an asymmetric kinase-competent state. Overall, the known structural changes of the sensor kinase, as well as further dynamic rearrangements that we now predict, consistently link structure determinants to activity modulation.

Accepted 6 July, 2015. *For correspondence. E-mail albanesi@ibr-conicet.gov.ar, demendoza@ibr-conicet.gov.ar; Tel. 54-341-4237070; Fax 54-341-4390465. †Co-first author.

Introduction

Propagation of a signal through transmembrane segments of sensor proteins is at the very basis of many complex signaling processes. However, little is known about the molecular nature of this important event. In this work we present a model for transmembrane signaling of DesK, a thermosensory protein from *Bacillus subtilis* activated by cold temperatures. The thermosensor DesK, which constitutes a canonical two-component system together with the response regulator DesR, has been extensively studied (Aguilar *et al.*, 2001; Cybulski *et al.*, 2002; Albanesi *et al.*, 2009; Trajtenberg *et al.*, 2010; 2014; Martin and de Mendoza, 2013, for a recent review, see de Mendoza, 2014).

Several biophysical evidences support the idea that upon lowering the environmental temperature lipid bilayers will become more ordered and as a consequence they will become thicker (Leonenko *et al.*, 2004; Pan *et al.*, 2008; Szekely *et al.*, 2011; Jambeck and Lyubartsev, 2012). Indeed, *in vivo* and *in vitro* experiments have suggested that DesK senses the thickening of the membrane as the temperature drops, resulting in a conformational change that triggers its autokinase activity (Cybulski *et al.*, 2010; Martin and de Mendoza, 2013; Porrini *et al.*, 2014). Subsequently, phosphorylated DesK activates DesR, a transcriptional activator of the *des* gene, coding for a Δ5-fatty acid desaturase (Δ5-Des). Unsaturated fatty acids, products of Δ5-Des, eventually promote a more fluid membrane that would switch DesK back from a kinase to a phosphatase state. Consequently phospho-DesR declines and transcription of the *des* gene is terminated (Fig. S1) (Aguilar *et al.*, 2001; Albanesi *et al.*, 2004; 2009).

DesK has an N-terminal domain composed of 5 transmembrane (TM) helices, with the last one extending into the cytoplasmic side (Fig. 1A) (Cybulski *et al.*, 2010). DesK is devoid of any extracellular domains and its cytosolic portion (DesKC) displays the characteristic homodimeric structure observed in other proteins of the family. Each DesKC monomer consists of an N-terminal antipar-

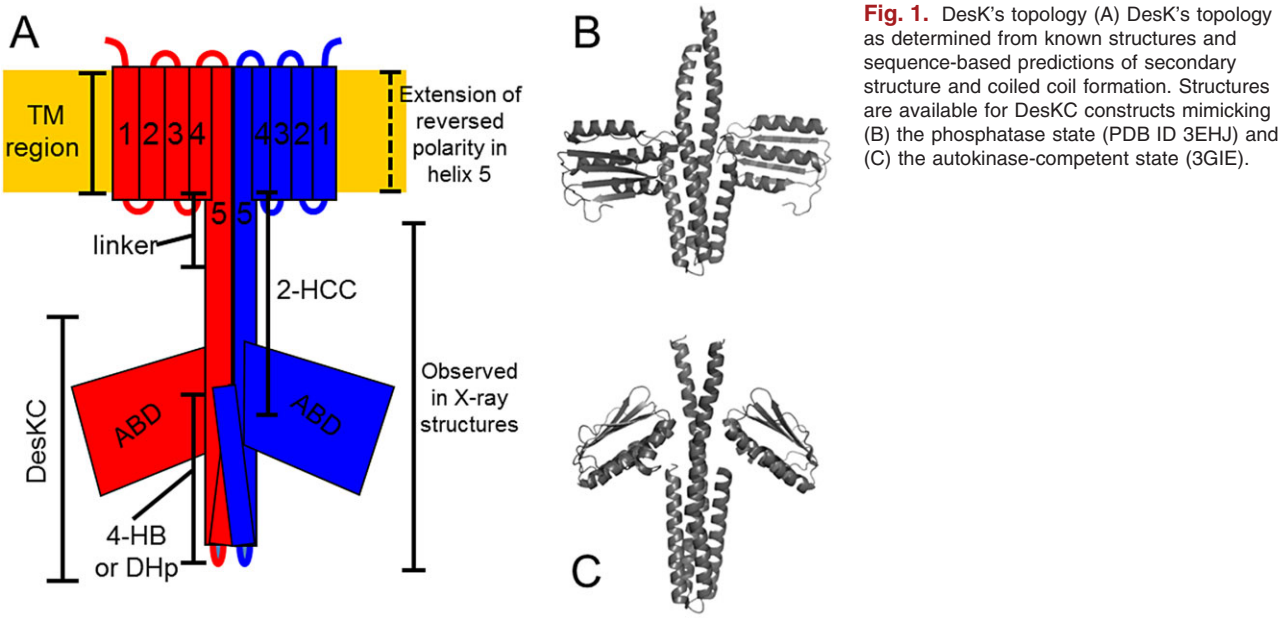

Fig. 1. DesK's topology (A) DesK's topology as determined from known structures and sequence-based predictions of secondary structure and coiled coil formation. Structures are available for DesKC constructs mimicking (B) the phosphatase state (PDB ID 3EHJ) and (C) the autokinase-competent state (3GIE).

allel 2-helix hairpin (helices α1 and α2) that includes the phosphorylatable histidine (His188), connected by a short loop to a C-terminal ATP-binding domain (ABD) (Albanesi *et al*., 2009). The helical hairpins of two monomers interact with each other to form a central four-helix-bundle (4-HB) domain, known as the DHp (Dimerization and Histidine phosphotransfer) domain. In each monomer, the N-terminal end of helix α1 extends beyond the 4-HB, connecting the catalytic core with the TM sensor domain through a helical linker (Albanesi *et al*., 2009). The amino acid sequences of helices α1 and α2 follow a heptad repeat pattern (with amino acids occupying positions *a* through *g*) with hydrophobic residues at positions *a* and *d* (Fig. S2) (Albanesi *et al*., 2009), characteristic of coiled coil domains (Crick, 1953a).

Replacement of His188 by a valine in DesKC results in a protein locked in the phosphatase state characterized by a tight packing of the DHp and ABD domains and by the formation of a parallel 2-helix coiled coil (2-HCC), as seen in the corresponding X-ray structures (Albanesi *et al*., 2009). This 2-HCC has been observed in many HKs, typically preceding the 4-HB (Singh *et al*., 1998), and corresponds more generally to the signaling helix, or 'S-helix', that connects helical sensor and effector domains in a wide range of signaling proteins (Anantharaman *et al*., 2006). This organization is indeed conserved in the phosphatase state of DesK, whose 2-HCC extends outward from the 4-HB toward the TM domain (Albanesi *et al*., 2009) ending right before the helical linker mentioned above (Fig. 1B). In contrast, the conformation corresponding to the kinase-competent state is less compact (Fig. 1C). The helices protruding from the 4-HB toward the TM domain are not packed in a coiled coil, and the ABD domains are dissociated from the 4-HB (Fig. 1C). Extensive structural characterization of the functional states of DesK led to a mechanistic signal transmission hypothesis (Albanesi *et al*., 2009) in which formation and disruption of the 2-HCC is a key step for shifting the output phosphatase/kinase ratio. Capable of transmitting the necessary conformational changes, this 2-HCC switch could modulate the exposure of the phosphorylatable histidine, as well as the toggling of intramolecular rigid/free DHp-ABD association.

Under such a mechanism, in the context of a fluid membrane, the TM domain would stabilize the connecting 2-HCC and the catalytic core in a compact, rigid conformation with the ABDs attached to the DHp domain. This conformation inhibits the autokinase activity, and the DHp surface is competent to interact with phospho-DesR. Upon cold signal reception, the 2-HCC would be disrupted and the ensuing structural reorganization would release the ATP binding domains for histidine phosphorylation resulting in a kinase-on state (Albanesi *et al*., 2009). Here we report experiments demonstrating that mutations that either stabilize or destabilize the 2-HCC displace the conformational equilibrium of full-length DesK toward constitutive phosphatase- or kinase-competent states respectively. Computational approaches further explain our experimental results and extend deeper insights into the signaling mechanism itself, in terms of a rearrangement of the TM helices triggered by a change in membrane properties.

Results

Functional relevance of the parallel 2-helix coiled coil for DesK signaling

The X-ray structure of $DesKC_{H188V}$ (PDB 3EHJ) shows a 2-HCC with clear electron density spanning residues 163 to 180, whereas the N-terminal residues 153 to 162 are poorly defined. Coil prediction servers [COILS, PCOILS (Lupas *et al*., 1991; Lupas, 1996)] consistently suggest that the 2-HCC actually extends all the way from the DHp domain through the entire linker region toward the N-terminus up to the C-terminus of the fifth TM helix (TM5). Secondary structure predictions further suggest that the helical structure continues as such through the membrane. If the coiled coil extends all along TM5, the hydrophobic side-chains are predicted to point outward in this TM segment, exposed to the hydrophobic membrane milieu, whereas a few polar residues would make contacts across the two helices (DesK's sequence is shown in Fig. S2 and sequence-based predictions for the first 120 residues of TM5-DesKC are summarized in Fig. S3). Therefore, in the phosphatase state, the two helices protruding from the DHp toward the membrane very likely assemble into a 2-HCC all the way up to, and through the membrane, as later modeled (see below).

To test the hypothesis that the 2-HCC organization is a determinant of the phosphatase state that is loosened in the autokinase-competent form and that this modulation is a basis of the signal transduction mechanism, we built and tested *in vivo* DesK structure-based mutants designed to weaken or favor the formation of the 2-HCC. In addition, we also analyzed a mutant aimed at disrupting the interdomain DHp–ABD association, as a supplemental mechanism for shifting the conformational equilibrium between phosphatase- and kinase-competent forms. These mutations fall in three classes: (i) changes in the 2-HCC (Ala167Arg, Ile171Gly, Leu174Gly) where polar and neutral residues are introduced at the '*a*' and '*d*' positions of the heptad repeats to disrupt the hydrophobic interactions of the 2-HCC (mutant dubbed $DesK_{DEST}$) (Fig. S2); (ii) introduction of substitutions (Ser150Ile, Ser153Leu, Arg157Ile, also predicted to occupy position '*a*' and '*d*' on the heptad repeats) to stabilize a 2-HCC structure toward the N-terminal domain of DesK, precisely where TM5 exits the inner leaflet of the membrane ($DesK_{STA}$) (Fig. S2); and (iii) a third mutant (Phe346Ala, Asn348Ser) named $DesK_{DHp\text{-}ABD}$ aimed at disrupting some of the main interactions between the DHp and ABDs domains in the phosphatase state (Fig. S2).

We engineered *desK*$^-$ cells of *B. subtilis* DAK3 and AKP20 strains, suited to probe kinase and phosphatase activity respectively (see *Experimental procedures*), to express the DesK variants in response to an inducer (Fig. S4). To monitor the signaling states of the point mutants, we used a reporter assay that is sensitive to changes of DesK activity *in vivo* (Aguilar *et al*., 1999; 2001; Cybulski *et al*., 2002; Porrini *et al*., 2014). To this end, we assayed the levels of β-galactosidase activities as encoded by a *lacZ* reporter gene fused to the desaturase promoter, which is activated only when there is flux of phosphate from DesK to DesR (Aguilar *et al*., 2001; Cybulski *et al*., 2004). Figure 2 compares the kinase activities for the mutant variants to wild-type (WT) activity in DAK3, and Supplementary Fig. S5 records the phosphatase activities for these variants in AKP20. We found that mutations expected to weaken the 2-HCC ($DesK_{DEST}$) or the DHp-ABD association ($DesK_{DHp\text{-}ABD}$) exhibited both, at 25°C and 37°C, β-galactosidase activity levels ~12-fold higher than the ones obtained with WT DesK at 25°C (Fig. 2), implying a favored kinase state of the sensor regardless of the temperature signal. As shown in Fig. S5, these strains maintain a phosphatase-off state. In addition, we found that mutations contained in $DesK_{STA}$ produce a kinase-off state and a phosphatase-on state *in vivo* (Fig. 2 and Fig. S5), as expected according to our proposed model for the stabilization of the connecting coiled coil. Altogether, the mutational studies provide strong evidence in support of the role of 2-HCC as a switch that transmits the temperature signal to the catalytic domain. This analysis also demonstrates that the contacts between the DHp and ABD domains are essential in controlling the activities of the sensor, in agreement

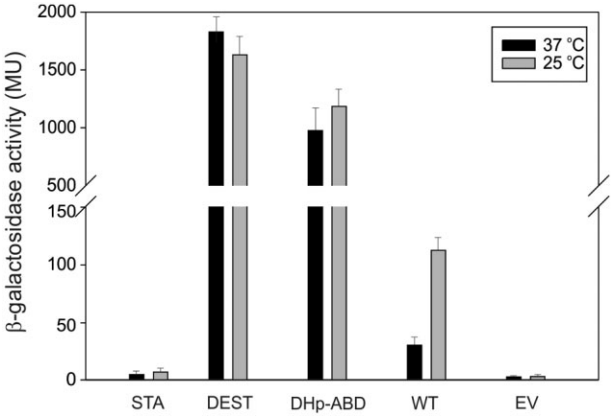

Fig. 2. *In vivo* kinase activity of DesK mutants. Strain DAK3 (*desK::km* P*xyl-desR amyE*::P*des-lacZ*) was complemented in *trans* with $desK_{DEST}$ (DEST), $desK_{STA}$ (STA), $desK_{DHp\text{-}ABD}$ (DHp-ABD) or wild type DesK (WT) under the control of the xylose inducible promoter Pxyl, or transformed with the empty vector pHPKS (EV). The strains were grown overnight in SMM-CAA in the absence of xylose and then diluted in the same medium to a final $DO_{525} = 0.12$. 0.1% xylose was added and the cultures were grown at 37°C with shaking. At $DO_{525} = 0.3$, each culture was divided in two and one half was kept at 37°C, whereas the other was transferred to 25°C. β-galactosidase specific activities were determined 4 hours after transferring the cells to the indicated temperatures. Data are represented as mean ± SD. MU, Miller units.

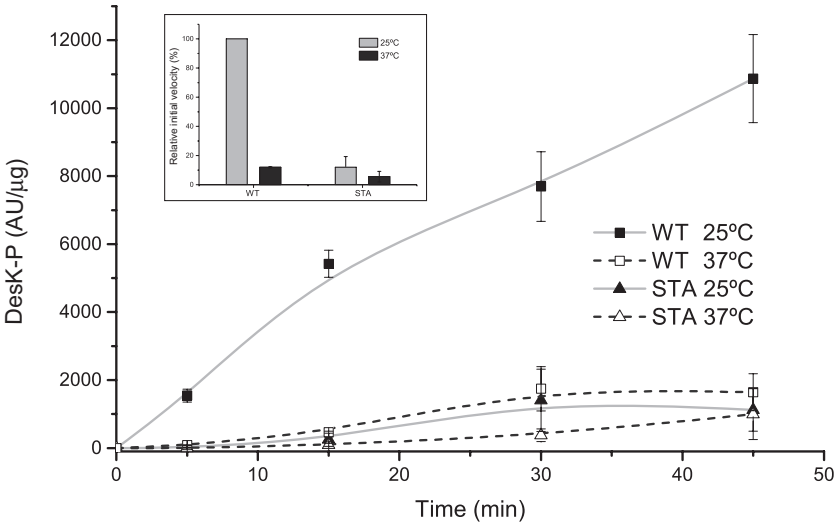

Fig. 3. Autophosphorylation of WT DesK and $DesK_{STA}$ inserted into liposomes. Purified WT DesK and $DesK_{STA}$ reconstituted into liposomes of *E. coli* polar lipids were incubated with [^{32}P-γ] ATP at 25°C (filled symbols) or 37°C (open symbols) and analyzed as described in *Experimental procedures*. The total amount of WT DesK~P or $DesK_{STA}$~P (AU) present in each well was determined by densitometry and plotted as AU/μg protein vs time. DesK (squares), $DesK_{STA}$ (triangles). Inset: Relative initial velocity of autophosphorylation of WT DesK (left) and $DesK_{STA}$ (right) in liposomes at 25°C (gray columns) and 37°C (black columns). The initial velocity of WT DesK at 25°C was considered as 100%. Data are represented as mean ± SEM. Autoradiography films representative of each phosphorylation assay are shown in Fig. S8.

with *in vitro* studies on the cytosolic domain of the histidine kinase HK853 from *Thermotoga maritima* (Marina *et al.*, 2005).

Effect of temperature on $DesK_{STA}$ activities

The *in vivo* studies clearly indicated that $DesK_{DEST}$ and $DesK_{DHp\text{-}ABD}$ are locked in a kinase-dominant state, both at 37°C and 25°C. However, some questions remained concerning the activity of $DesK_{STA}$ at 25°C because (i) no β-galactosidase activity was detected at low temperature for this variant in the kinase assay in DAK3 and (ii) strain AKP20 only allows to test for the phosphatase activity of the proteins but not for regulation of this activity by temperature. This is due to the high levels of Δ5-unsaturated fatty acids synthesized by strain AKP20 (Altabe *et al.*, 2003) that are known to promote the phosphatase activity of DesK (Aguilar *et al.*, 2001). Therefore, to gain further information on the influence of temperature on the activities of $DesK_{STA}$ and provide a solid biochemical ground to our mutational analysis, we studied the autokinase and phosphatase activities of WT DesK and $DesK_{STA}$ reconstituted into liposomes formed by *Escherichia coli* phospholipids. These lipids undergo a reversible change of state from a fluid to a non-fluid array of fatty acyl chains when the temperature is decreased from 37°C to 25°C, instrumental for this analysis (Martin *et al.*, 2009). On the one hand, we found that the autokinase activity of $DesK_{STA}$ was much lower than that of WT DesK, both at 37°C and 25°C (Fig. 3), exhibiting at 25°C comparable levels of kinase activity to WT DesK at 37°C. These data agree with the *in vivo* assays indicating that $DesK_{STA}$ is in a kinase-off state. On the other hand, consistent with our proposition that $DesK_{STA}$ is in a phosphatase-on state, this protein was able to dephosphorylate phospho-DesR at higher rates than WT DesK, both at 25°C and 37°C (Fig. 4), exhibiting at 25°C comparable levels of phosphatase activity to WT DesK at 37°C. These data, combined with the *in vivo* analysis, provide compelling evidence supporting a model in which a reversible formation of the membrane-connecting 2-HCC regulates the balance of phosphatase and kinase activities of full-length DesK.

Driving force for stabilization and destabilization of the 2-helix coiled coil

To gain further mechanistic insights, we built *in silico* atomistic models of WT DesK starting from its TM5 (TM5-DesKC, shown in Fig. 5B) as well as of the two 2-HCC variants (TM5-$DesKC_{STA}$ and TM5-$DesKC_{DEST}$, Fig. 5A and C, respectively). The models were embedded in atomistic membranes, surrounded with explicit water and relaxed through ~55 ns of molecular dynamics (MD) simulations.

By design, at the beginning of the calculations, the three models shared exactly the same backbone conformation, i.e. that of a perfect coiled coil (Fig. 5B). Upon equilibration to 27°C (~1 ns) Pro148 kinks in all three models due to steric clashes between the bulky side-chains of Leu146 and Leu147, which interact among monomers. In both WT TM5-DesKC and TM5-$DesKC_{DEST}$, this slightly opens up the coiled coil (insets in Fig. 5B and C) allowing a few water molecules to interact with the polar residues of the segment 146–157 containing Ser150, Ser153 and Arg157 (Fig. 5B and C). This hydrated status is maintained along the 50 ns of both simulations. In contrast, no water molecules are seen to penetrate in the stabilized variant TM5-$DesKC_{STA}$, during the 50 ns of simulation, consistent with the engineered hydrophobic residues acting as a greasy cap that stabilizes the coiled coil (Fig. 5A).

In TM5-$DesKC_{DEST}$, substitutions Ala167Arg, Ile171Gly and Leu174Gly further lead to increased hydration of the segment 167–174, which is instead barely hydrated in WT

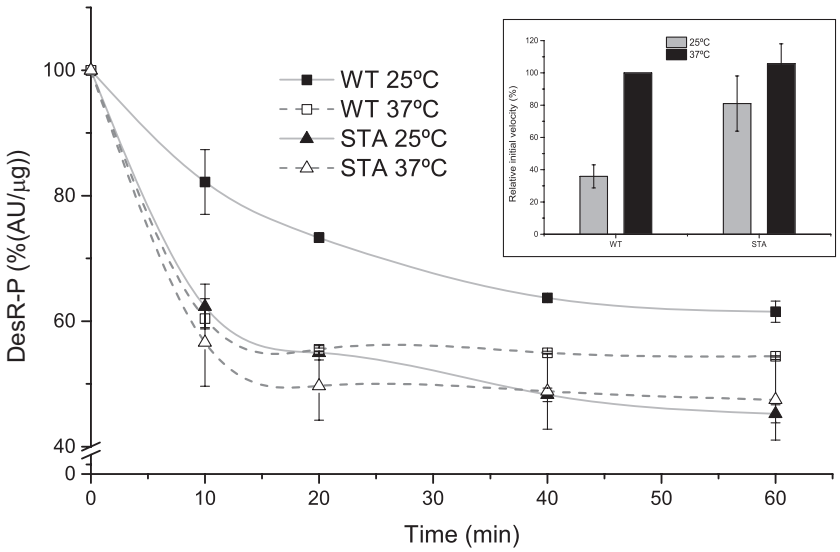

Fig. 4. Dephosphorylation of DesR~P by WT DesK and $DesK_{STA}$. DesR~P was purified as indicated in *Experimental procedures* and incubated with proteoliposomes of WT DesK (squares) or $DesK_{STA}$ (triangles) at 25°C (filled symbols) or 37°C (open symbols). Aliquots were withdrawn at several times and analyzed by SDS-PAGE as described in *Experimental procedures*. The intensity of the bands corresponding to DesR~P at each time point were determined by densitometry and plotted as the % of remaining DesR~P/µg protein vs. time, considering the intensity of the band of DesR~P at the initiation of the reaction (0 min) as 100% of DesR~P. Inset: Relative initial velocity of phosphatase activity of WT DesK (left) and $DesK_{STA}$ (right) proteoliposomes at 25°C (gray columns) and 37°C (black columns). The initial velocity of WT DesK at 37°C was considered as 100%. Data are represented as mean ± SEM. Autoradiography films representative of each dephosphorylation assay are shown in Fig. S8.

TM5-DesKC and TM5-$DesKC_{STA}$ (Fig. 5). These results support our initial mutagenesis design and our hypothesis that compacting forces stabilize the 2-HCC, further suggesting that stabilization/destabilization of the 2-HCC is linked to the hydration state of the region where the protein inserts into the membrane (just C-terminal to Pro148).

Modeling the 2-HCC in the context of a full minimalistic working protein

The results presented here show that stabilization/destabilization of DesK's 2-HCC on its cytoplasmic side is essential for cold sensing. However, linking this finding to other available functional evidence to make further interpretations and speculate about how 2-HCC rearrangements could be triggered and transmitted by the TM region is hampered by the lack of structures or models of full-length DesK. Therefore, we focused on a minimalist but fully functional DesK surrogate dubbed MS-DesK (Cybulski *et al*., 2010) in which the first half of DesK's first TM helix is fused to the second half of DesK's fifth TM helix forming a long continuous helix plugged into the 4-HB. Capitalizing on this simple single-membrane-pass helical topology (Fig. S2), we proceeded to model MS-DesK *in silico*. Specifically, and taking into account that DesK would be activated by membrane thickening, we built models of the minimal sensor in the phosphatase and autokinase-competent states and relaxed them through ~120 ns of MD simulations (Fig. 6A) in DOPC (1,2-di-(9Z-octadecenoyl)-*sn*-glycero-3-phosphocholine) and DEPC (1,2-dierucoyl-*sn*-glycero-3-phosphocholine) membranes, the latter being ~4.5 Å thicker (Mathai *et al*., 2008; Xu *et al*., 2008; Muhle-Goll *et al*., 2012). When modeling these structures, we took into account that each helix of the 2-HCC extends as a continuous element into the TM region according to secondary structure predictions, interrupted only by Gly13 and Pro16, and that the two helices need to pair their polar residues in the TM region so as to hide them from the hydrophobic membrane portion (Deber and Ng, 2015; Zhang *et al*., 2015).

Modeling MS-DesK in the phosphatase state by extending the portion of 2-HCC observed in PDB ID 3EHJ with the sequence of the minimal sensor and canonical coiled coil parameters, as done for TM5-DesKC, was straightforward. In a DOPC membrane, this relaxes into a stable 2-HCC through the cytosolic and most of the TM region with a slight hydration of the 146–157 segment, as described for WT and destabilized TM5-DesKC. Gly13, one helix turn on top of Pro16, acts as a hinge that allows the small N-terminal helical segment to fully hydrate exposing the internal polar residues to the solvent [Fig. 6A(i) and S6A, C]. In contrast, in the thicker and less fluid membrane composed of DEPC, no opening of the N-terminal region is observed, and the 2-HCC remains paired also in the first half of the transmembrane region [Fig. 6A(ii)].

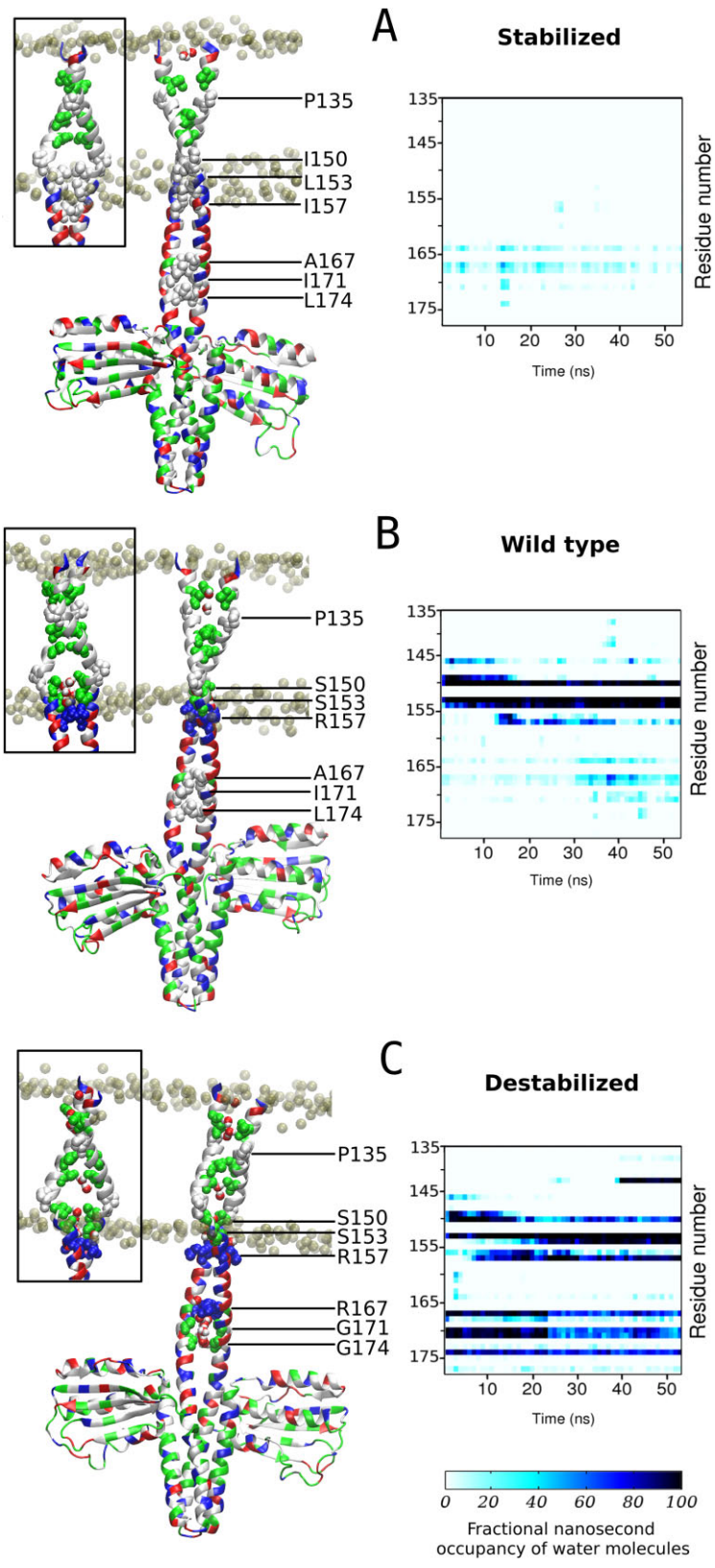

Fig. 5. Stability of wild type, stabilized and destabilized variants of TM5-DesKC. Models (A = $DesK_{STA}$, B = wild type, C = $DesK_{DEST}$) were built for the three variants embedded in DOPC membranes in explicit water, and simulated with molecular dynamics. On the left side, final snapshots from the simulations showing the backbone in cartoon representation and selected residues rendered as spheres, colored by amino acid type as defined in the VMD program (gray = hydrophobic, green = polar uncharged, red = negatively charged and blue = positively charged). The insets are ~90° rotations around the membrane normal. On the right side, plots showing the time progression of internal 2-HCC hydration quantified as the fractional nanosecond occupancy of water molecules contacting simultaneously both helices of the 2-HCC.

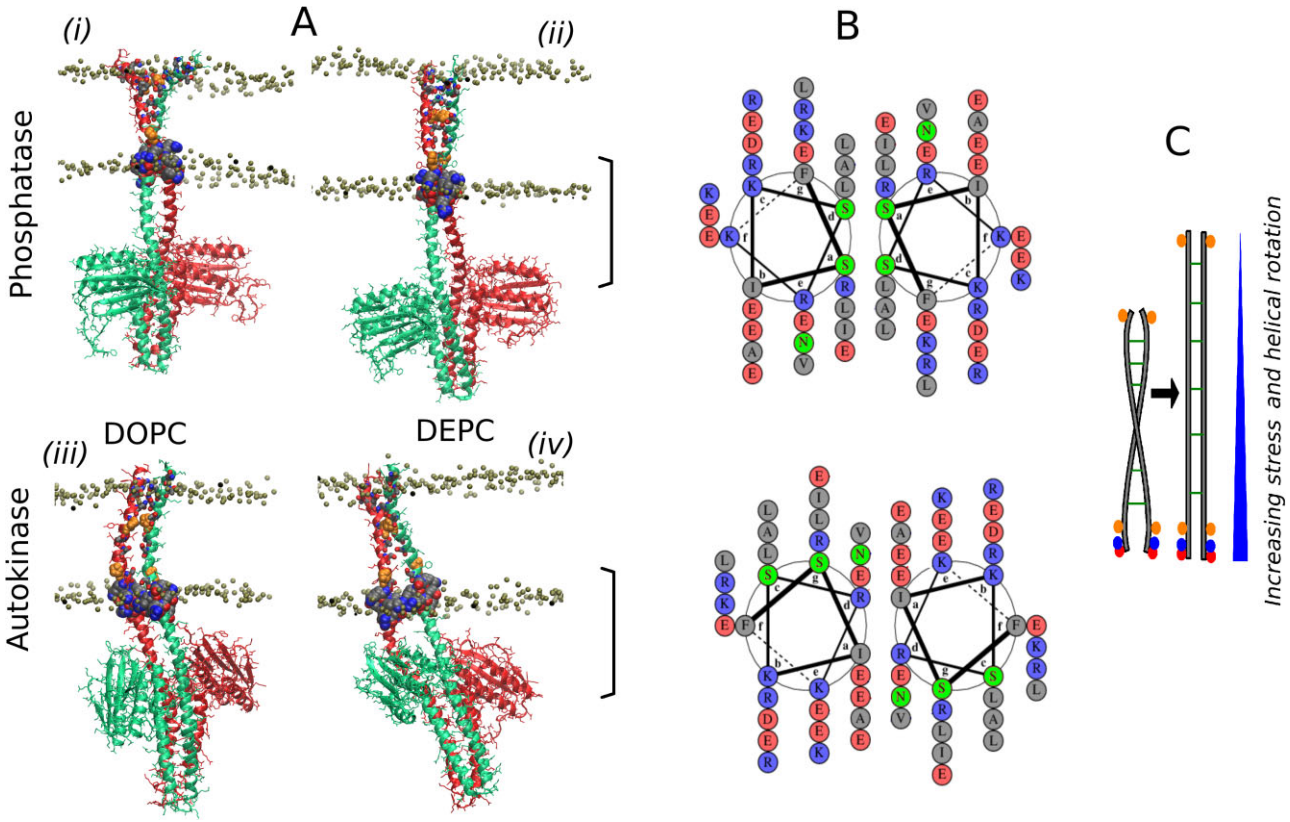

Fig. 6. Models of MS-DesK in the phosphatase and kinase states, relaxed in two membranes of different thickness. Models were built from the X-ray structures of DesKC in the phosphatase and autokinase-competent state (PDB ID 3EHJ and 3GIE, respectively) by extending their helices towards their N-termini following the sequence of MS-DesK. Each model was relaxed through 120 ns of MD simulation in a DOPC or DEPC membrane as indicated, in explicit solvent. Heavy atoms from the KERER segment are rendered as blue, red and gray spheres (N, O and C, respectively) while all heavy atoms of the two prolines of the TM region (Pro135 and 148) were rendered in orange. Panel (B) shows helical wheel diagrams (Grigoryan and Keating, 2008) between Phe149 and the entry to the 4-HB, with polar uncharged residues in green, negative residues in red and positive residues in blue. Panel (C) sketches the idea that unwinding of the 2-HCC results in rotation of the helices between the two Pro residues (in orange) as the membrane thickens, highlighting also that the KERER segment (red and blue spheres) does not shift along the membrane normal when it changes thickness.

Modeling MS-DesK in the autokinase-competent state was more complicated because the 2-HCC segment resolved in the starting structure (PDB ID 3GIE) has many non-canonical interactions due to helical displacements and rotations relative to the phosphatase form, features deemed functional within scissoring, rotation and tilting mechanisms of DHp activation (Lemmin *et al.*, 2013; Molnar *et al.*, 2014). Under the restraint that the polar residues located in the very hydrophobic segment of the helices (Thr140 and Ser143) should pair back in the transmembrane portion (Deber and Ng, 2015; Zhang *et al.*, 2015), the model ends up adopting stretched, nearly parallel TM helices, instead of a coiled coil arrangement [Fig. 6A(iii), (iv) and S6B, D], like in two nearly full structures of histidine kinases in their kinase-competent forms (Fig. S7) (Diensthuber *et al.*, 2013; Wang *et al.*, 2013). Upon relaxation in either kind of membrane, this model experiences asymmetric distortions and cracking of one helix close to the 4-HB, which reflect a stressed, dynamic conformation of the parallel coil in this activated state, as very recently proposed for other histidine kinases (Dago *et al.*, 2012; Diensthuber *et al.*, 2013; Wang *et al.*, 2013; Casino *et al.*, 2014; Mechaly *et al.*, 2014).

From the contacts observed across subunits for residues in the models of MS-DesK in the kinase and phosphatase states (Fig. 6A), we have sketched helical wheel diagrams (Grigoryan and Keating, 2008) that summarize key aspects and differences of the 2-HCC in its two states (Fig. 6B). We have constructed these diagrams between residue Phe149, which defines the end of the hydrophobic portion of TM5 and residue Arg180 right at the entry of the 4-HB. In the phosphatase form, the phenylalanine is at position 'g' of the coiled coil's heptad pattern, just as predicted from the sequence alone (Fig. S2). The first two helical turns seen in these plots, which are right before quitting the membrane, are stabilized by hydrogen bonds between serine residues (S143, S150) across helices. Next toward the C-terminus, in the inner polar region of the

membrane and into the cytoplasm, the 2-HCC is stabilized by internal hydrophobic contacts while all charged residues remain exposed to the solvent. In the kinase form, instead, the roughly 90° rotation of each helix results in the exposure of several hydrophobic residues and the burial of large charged residues inside the coil, which is precisely opposite to what one expects for proteins in solution, implying a stressed conformation. The heptad repeat pattern is displaced by one position, with Phe149 being now at position 'f' which is roughly one quarter of a helix turn, i.e. 90°.

We finally highlight that relaxation of the models embedded in membranes shows that the highly charged segment just C-terminal to the TM region (K^{152}SRKERERLEEK^{163}, Fig. S2) remains in the four cases anchored to the cytoplasmic polar side of the membrane.

Discussion

Our *in vivo* and biochemical experiments, structural analyses and simulations, demonstrate that stabilization/destabilization of a 2-HCC is directly involved in regulating DesK's functional state. The portion of the 2-HCC that connects the transmembrane region to the DHp domain corresponds to the 'signaling helix', or 'S-helix', a feature that is conserved between sensor and effector domains across a wide range of signaling proteins as a general signal-transduction element of long persistence length that can allow for the propagation of rotations and displacements over long distances (Anantharaman *et al*., 2006; Moglich *et al*., 2009). The S-helix was proposed to organize into coiled coils that work as a stability switch that prevents constitutive activation of the catalytic domains (Anantharaman *et al*., 2006). Our findings now lend direct support to this role of the S-helix. Indeed, we observed that the stabilization of the 2-HCC favors the phosphatase state while preventing any autokinase activity, whereas the opposite occurs upon 2-HCC destabilization.

Additionally, our structural analyses and MS-DesK models show that interconversion of DesK functional states implies roughly 90° rotation of each helix of the 2-HCC (Fig. 6A and B), pointing to helical rotations as modulators of the 2-HCC stabilization/destabilization. Our simulations further suggest that the highly charged segment just C-terminal to the TM region (K^{152}SRKERERLEEK^{163}, Fig. S2) is strongly anchored to the cytoplasmic polar side of the membrane. This anchor could be important to limit movements of the TM and 2-HCC helices when the membrane properties change, allowing them to rotate and possibly hinge, tilt and stretch, but preventing them from sliding along the membrane normal. A previous work suggested that this segment undergoes a helix/random coil transition at the heart of the sensing mechanism (Inda *et al*., 2014), a hypothesis that goes against all evidence supporting the role of the S-helix in histidine kinases. Our newly proposed mechanism does not require a helix/random coil transition and is consistent with the S-helix hypothesis. In summary, we favor a mechanism based on transitions of the TM region between a 2-helix coiled coil in the phosphatase form and two parallel helices in the kinase form, linked to internal helical rotations.

Origin of the primary signal that promotes rotation of the 2-HCC helices

Available structural data have revealed several features of the DHp domain rearrangements that control the output catalytic behavior of several histidine kinases (Bhate *et al*., 2015). However, it is still poorly understood how input signals get transduced into these DHp rearrangements, which might depend on the specific sensor domains, the transmembrane region and the DHp family (Finn *et al*., 2014). DesK represents an excellent model to study signal generation and transduction given the amount of structural and functional information available, its lack of extracellular and HAMP domains, and the fact that the last TM helix continues smoothly as an S-helix-like element into the DHp domain.

According to our results and as discussed above, the activation signal sensed by DesK must ultimately promote rotation of the 2-HCC to destabilize it. In sensor domains sensitive to different signals, particular triggers would promote helical rotations at the 2-HCC. In the case of DesK, experimental evidence suggests that these triggers would be mechanical inputs from the membrane. More precisely, *in vivo* and *in vitro* studies suggested that the initial mechanical trigger for the activation of DesK and MS-DesK is a thickening of the membrane, because (i) the proteins exhibit increasing kinase activity when reconstituted into vesicles of longer acyl chains (Cybulski *et al*., 2010; Martin and de Mendoza, 2013) and (ii) DesK kinase activity is stimulated in bacteria with a higher proportion of long-chain fatty acids in their membranes, whereas an increment in the amount of short-chain fatty acids stimulates its phosphatase activity (Porrini *et al*., 2014). As mentioned above, the thickness difference of the lipid bilayers used in previous *in vitro* experimental tests and in the simulations presented here is ~4.5 Å. This does not necessarily mean that a change of this magnitude could take place in a bacterial membrane when it transitions from 37°C to 25°C. However, recent work from our laboratory suggests that *in vivo* DesK would be activated by the fluid phase-to-gel transition, what could result in a greater increase in bilayer thickness upon a temperature downshift (Martin and de Mendoza, 2013).

Our models allow us to propose that, from the protein side, the initial signal is a stretching of the helices combined with helix tilting, as required to maintain hydrophobic matching to the membrane. Such stretching and tilting could be induced either directly by thickening of the membrane and/or by other membrane properties that vary together with thickness, such as fluidity/stiffness and water permeability (Kucerka *et al*., 2005; Zhang and Rock, 2008; Blicher *et al*., 2009; Lee, 2011). Membrane thickness and fluidity are well-known to affect the orientation and conformation of transmembrane proteins (Lee, 2003; 2004), whereas water permeability could be particularly important in the case of DesK given our experimental and computational results mainly on the stabilized DesK variant where hydration of the 2-HCC is precluded (Fig. S6). We notice finally that it would be difficult to disentangle either through experiments or simulations the contributions from changes in the different membrane properties.

A stretching of the 2-HCC in the TM region implies unwinding of the canonical coiled coil, keeping the internal polar contacts between helices in the TM regions. This results in helix tilting to achieve a lower helix-crossing angle [~25° in the phosphatase state against ~5° in the kinase state according to the models, comparable with a difference of 16° in another system (Diensthuber *et al*., 2013)] and a rotation of the helices around their main axes toward the cytosolic side that must reach ~90° by Phe149 according to the X-ray structures and models (Fig. 6B). We propose such rotation arises as the conversion of the stress released upon stretching of the coiled coil in its TM region into a torque (Fig. 6C), although we cannot rule out other direct effects from, for example, helix tilting.

Toward a full mechanism for cold sensing by DesK

The following mechanism emerges from the ideas developed above for signal sensing and transduction by DesK. A temperature drop results in thickening of the membrane and pairing of the 2-HCC in its outer side. As the membrane thickens, the TM segment is stretched from its ends. This stretching induces unwinding of the 2-HCC and a gradual rotation of its helices increasing downstream toward the cytoplasmic side, reaching 90° by the KERER segment where the 2-HCC exits the TM region. The 90° rotation is transmitted to the 2-HCC bringing large charged residues to its interior, which forces its destabilization and separation of its helices. The resulting helix rotation and separation are transmitted to the DHp's 4-HB, which now hides the residues that were generating an extensive DHp–ABD interaction surface in the phosphatase form (Albanesi *et al*., 2009) thus releasing the ABD domains and promoting the kinase state.

Besides the direct evidence from mutations that stabilize/destabilize the 2-HCC as presented here, previous experimental results on other mutants support or can be reinterpreted in terms of our proposed mechanism. The opening/closing or hydration/dehydration of the N-terminal external segment of MS-DesK has been independently postulated from mutational evidence (Cybulski *et al*., 2010), now explained by the models to be related to the hinge at Gly13-Pro16. On the cytoplasmic side, charge-neutralizing substitutions in the K^{155}ERERLE segment showed that removing the positive charges (Arg or Lys replaced by Ala) enhances MS-DesK's cold-sensing capacity (i.e. favors the kinase state), whereas removing the negative residues (Glu to Gln substitutions) abolishes it (Inda *et al*., 2014). In the context of our models and mechanism, when the negative residues are replaced by glutamine, there would be a stabilization of the coiled coil, thus decreasing kinase output, because repulsion of the glutamates from both helices is removed and most importantly, because several hydrogen bonds can be formed. Instead, when the positive charges are replaced by alanine, the region acquires a high net negative charge with no screening by positive charges and no stabilizing bonds, pushing the helices apart and thus destabilizing the coiled coil into the kinase state. Finally, single-point substitution of the three Ser residues of the TM region by alanine (S143, S150 and S153, of which the last two are in the final helix turn before leaving the membrane) have been reported to decrease the kinase activity of MS-DesK (Cybulski *et al*., 2015). This effect was originally interpreted in terms of a 'serine zipper' model. Our models are consistent with that proposal, but so that the zip is mediated by 90° helical rotations such that the serines are zipped together in the phosphatase state and open (i.e. rotated away) in the kinase state (Fig. 6B). In this scenario, the effect of substituting these serine residues, especially Ser150 and Ser153, by alanine, is similar to that of our coiled-coil stabilizing variant (i.e. stabilizing the 2-HCC and thus the phosphatase form). Moreover, this mechanism explains also why the reported serine-to-alanine replacements do not fully impair the kinase activity as observed for $DesK_{STA}$: single substitutions and the fact that alanine is less hydrophobic than leucine and isoleucine, result in less compaction of the 2-HCC. Altogether, these observations agree with the idea that a delicate balance must exist in the surface of the transduction element, i.e. the 2-HCC, to allow for the conformational transition to occur upon signal detection (Anantharaman *et al*., 2006; Liu *et al*., 2014). A too stable or a too weak coiled coil would lock the protein in a permanent OFF or ON state, respectively, making it insensitive to the signal, as observed with the $DesK_{STA}$ and $DesK_{DEST}$ variants.

In summary, we propose that membrane inputs related to cold-induced thickening trade off with the pro-

tein's internal mechanics, particularly those about 2-HCC stability and its helical rotations. Upon a drop in temperature the membrane becomes thicker and more structured, imposing on the 2-HCC a stress that results in its conversion from the relaxed phosphatase state [Fig. 6A(i)] into the autokinase-competent state [Fig. 6A(iv)]. Such mechanism explains several observations on DesK and MS-DesK and puts together essential components of signal transduction by histidine kinases, providing in turn new elements to address the fundamental problem of dynamic helix interactions in transmembrane signaling.

Experimental procedures

Plasmid and strain construction

Plasmids were constructed using standard methods and amplified in *E. coli* DH5α and DH10β strains. In order to construct a *desK*$^-$ mutant strain possessing an isotopic copy of *desR* under the control of the xylose inducible promoter P*xyl*, we first cloned the kanamycin resistance casstette (*km*) of pJM114 (Perego, 1993) into the *Eco*RI and *Hin*cII sites of *desK*, which had been previously cloned into the pBluescript vector (Strategene), obtaining plasmid pAGK382. In this construct, the central 533 bp of *desK* are missing, and the *km* cassette is flanked by its 5′ and 3′ ends. Then, we amplified *desK::km* from pAGK382 by PCR using oligonucleotides DesK-KpnI (5′-AAGTGAGGTACCATTATGATTAAAAATC-3′) and DesKBS_DW (5′-ATAGGATCCGTCGACTATGTTTAT TTTGAATTATTAGG-3′) and digested the product of the reaction with *Kpn*I and *Hin*cII. The fragment containing the 5′ end of *desK* fused to *km* (5′*desK-km*) was purified and cloned into pCM18 (pBluescrit/P*xyl-desR*) (Mansilla, personal communication) digested with the same restriction enzymes, just upstream of P*xyl-desR*, obtaining plasmid pCMK382. pCMK382 was then linearized with *Sca*I and transformed into the *B. subtilis* strain AKP3 (JH642 *amyE::* P*des-lacZ cm*) (Aguilar *et al.*, 2001). Transformants were selected in Luria–Bertani (LB) (Sambrook *et al.*, 1989) agar plates supplemented with chloramphenicol and kanamycin, 5 μg μl^{-1} each. Transformants were genetically (PCR from genomic DNA) and phenotypically (no expression of P*des* at low temperature) checked to confirm the deletion of *desK*. The resultant strain was named DAK3 (JH642 *amyE::* P*des-lacZ cm desK::km*-P*xyldesR*).

To obtain $desK_{DEST}$, $desK_{STA}$ and $desK_{DHp\text{-}ABD}$, we performed site-directed mutagenesis onto WT *desK* ($desK_{WT}$) using mutagenic oligonucleotides and overlap-extension PCR (Ho *et al.*, 1989). The ORFs coding for $desK_{WT}$, $desK_{DEST}$, $desK_{STA}$ and $desK_{DHp\text{-}ABD}$ were finally amplified using oligonucleotides DesK_UPS and DesK_DWBK (Albanesi *et al.*, 2004) and cloned into the *Sal*I and *Kpn*I sites of pGES40 (Albanesi *et al.*, 2004) downstream of the P*xyl* promoter. Subsequently, the resultant plasmids were digested with *BamH*I and the P*xyl-*$desK_{WT}$, P*xyl-*$desK_{DEST}$, P*xyl-*$desK_{STA}$ and P*xyl-*$desK_{DHp\text{-}ABD}$ fragments were cloned into the replicative vector pHPKS (Johansson and Hederstedt, 1999). Finally, pHPKS/P*xyl-*$desK_{WT}$, pHPKS/P*xyl-*$desK_{DEST}$, pHPKS/P*xyl-*$desK_{STA}$ and pHPKS/P*xyl-*$desK_{DHp\text{-}ABD}$ were used to transform strains DAK3 (*desK::km*-P*xyl-desR amyE::*P*des-lacZ*) and AKP20 (*desK::km*-P*km-desR amyE::*P*des-lacZ*) (Aguilar *et al.*, 2001).

Membrane preparation and western blot analysis

Strains DAK3 and AKP20 transformed with pHPKS/P*xyl-*$desK_{WT}$, pHPKS/P*xyl-*$desK_{DEST}$, pHPKS/P*xyl-*$desK_{STA}$, pHPKS/P*xyl-*$desK_{DHp\text{-}ABD}$ or the pHPKS empty vector were grown overnight in LB medium supplemented with 1% glucose and then diluted in LB medium to a final DO_{600} = 0.1. The cultures were incubated at 37°C with shaking. At DO_{600} = 0.3, each culture was divided in two and one half was supplemented with 0.8% xylose. Cells where harvested 4 hours later and resuspended in lysis buffer (50 mM Tris-HCl pH 8, 300 mM NaCl, 1 mM DTT and 1 mM PMSF), incubated for 30 minutes at 37°C with 1 mM lysozyme, and disrupted by sonication. Cell debris were separated by centrifugation at 12 000 *g*, the membrane fraction was purified by centrifugation at 2 00 000 *g*, and the pellet was resuspended in lysis buffer supplemented with 20% glycerol. Membrane proteins (100 μg) were analyzed by SDS-PAGE and subjected to immunoblotting with specific antiserum anti-DesKC to detect the expression of WT DesK and the mutant variants.

β-galactosidase activity assays

Strain DAK3 (*desK::km*-P*xyl-desR amyE::*P*des-lacZ*) transformed with pHPKS/P*xyl-*$desK_{WT}$, pHPKS/P*xyl-*$desK_{DEST}$, pHPKS/P*xyl-*$desK_{STA}$, pHPKS/P*xyl-*$desK_{DHp\text{-}ABD}$ or the pHPKS empty vector was grown overnight in Spizizen minimal salts (Spizizen, 1958) supplemented with 0.5% glycerol, tryptophan and phenylalanine (50 μg of each ml^{-1}), trace elements (Harwood and Cuttings, 1990), and 0.05% casein hydrolysate (this medium was named SMM-CAA), in the absence of xylose and then diluted in the same medium to a final DO_{525} = 0.12. 0.1% xylose was added and the cultures were grown at 37°C with shaking. At DO_{525} = 0.3, each culture was divided in two and one half was kept at 37°C while the other was transferred to 25°C. β-galactosidase specific activities were determined 4 hours after transferring the cells to the indicated temperatures, as previously described (Mansilla and de Mendoza, 1997), and were expressed in Miller units (Miller, 1972). To assay the phosphatase activity of DesK variants, we used strain AKP20 (*desK::km*-P*km-desR amyE::*P*des-lacZ*) that exhibits constitutive expression of P*des*, and hence high β-galactosidase activity levels, due to DesR overexpression from the strong constitutive *kanamycin* promoter (P*km*) and its phosphorylation from small phosphor-donors or other kinases (Aguilar *et al.*, 2001). Expression in AKP20 of WT DesK or of a DesK variant that exhibits DesR~P phosphatase activity leads to a decrease in the β-galactosidase activity levels (Aguilar *et al.*, 2001; Albanesi *et al.*, 2004). AKP20 transformed with pHPKS/P*xyl-*$desK_{WT}$, pHPKS/P*xyl-*$desK_{DEST}$, pHPKS/P*xyl-*$desK_{STA}$, pHPKS/P*xyl-*$desK_{DHp\text{-}ABD}$ or the pHPKS empty vector was grown overnight at 37°C in SMM-CAA. Cells were collected and diluted in SMM-CAA to a final DO_{525} = 0.12 either in the presence or in the absence of 0.1% xylose and grown at 37°C with shaking. β-galactosidase activities were determined 4 hours after dilution, as previously described (Mansilla and de Mendoza, 1997). The specific activities were expressed in Miller units (Miller, 1972).

Protein expression and purification

The open reading frames coding for WT DesK and $DesK_{STA}$ were cloned into the *Nde*I and *Sal*I sites of the pET22b expression vector (NOVAGEN), and the resulting plasmids were transformed into *E. coli* BL21 (DE3) cells. Cells expressing the his-tagged recombinant proteins were grown in LB broth at 37°C with agitation to an $OD_{600} = 0.8$. The cultures were then shifted to 18–20°C, and protein expression was induced by addition of 0.2 mM isopropyl-β-D-1-thiogalactopyranoside (IPTG). After 18 hours, cells were harvested and resuspended in lysis buffer (50 mM Tris-HCl pH 8, 300 mM NaCl and 1 mM PMSF). Cells suspension was incubated for 30 minutes at 37°C with 1 mM lysozyme, and disrupted with an Emulsiflex™ C3 homogenizer (AVESTIN). Cell debris were separated by centrifugation at 12 000 *g* for 20 minutes, and the supernatant was recovered. The membrane fraction was purified by centrifugation at 200 000 *g* for 2 h, the pellet was resuspended in lysis buffer supplemented with 1 mM DTT and 0.2% Brij58 and incubated overnight at 4°C, with mild agitation, for membrane solubilization. Unsolubilized membranes were separated by centrifugation at 200 000 *g*, and the supernatant was diluted fourfold in lysis buffer supplemented with 1 mM DTT. Protein purification was performed with standard Ni^{+2} affinity chromatography using Ni-NTA agarose resin (Qiagen) and then dialyzed against an excess volume of 50 mM Tris-HCl pH 8, 200 mM NaCl, 1 mM PMSF, 0.2% Brij58 and 10% glycerol at 4°C. To determine protein concentration, purified samples were loaded into 12% poliacrilamide gels together with BSA standards ranging in quantities of 0.1 μg to 2 μg. Gels were stained with Coomassie brilliant blue and densitometry of bands was measured with ImageJ software. BSA standards were used to build the calibration curve and protein sample concentrations were calculated by interpolation.

Proteoliposomes preparation

Liposomes were prepared as described previously (Martin *et al*., 2009; Martin and de Mendoza, 2013). Briefly, 8 mg of *E. coli* polar lipids (Avanti Polar Lipids, USA) were resuspended in 300 μl chloroform : methanol mix (2:1) and dried in a nitrogen atmosphere. Complete drying was achieved by heating at 65°C under vacuum for 2 hours. Large multilamellar vesicles (LMVs) were generated by solubilizing lipids in 1 ml of hydration buffer (20 mM Tris HCl pH 8, 250 mM sucrose and 100 mM K_2SO_4) during 1 hour with agitation. Large unilamellar vesicles (LUVs) were obtained by submitting LMVs to 10 freeze–thaw cycles and extrusion through a 0.2 μm filter on an Avanti® miniextruder at 65°C, with over 20 passes. For protein integration, preformed LUVs were incubated 30 minutes with Triton X-100 0.24% at room temperature. Pre-purified proteins in Brij58 micelles were added at a molar ratio 1:800 (protein : lipids) and incubated for 1 hour at 4°C. Detergent removal was achieved by adsorption to polystyrene beads BioBeads® SM2 during 3 days at 4°C. To separate proteoliposomes of free proteins, a sucrose gradient ultracentrifugation was performed as described previously (Martin *et al*., 2009). Proteoliposome samples were analyzed by SDS-PAGE and protein quantification was performed as described in the protein expression and purification section. Finally, proteoliposomes were used for biochemical characterization.

Biochemical characterization

All phosphorylation assays were carried out in reaction buffer (50 mM Tris-HCl, pH 8, 200 mM NaCl, 1 mM DTT, 20% glycerol, 50 mM KCl and 1 mM $MgCl_2$). For the autokinase activity assays, each protein was incubated in reaction buffer supplemented with 25 μM ATP and 0.25 μCi μl^{-1} [γ-^{32}P] ATP (NEN Life Science Products) at 25°C or 37°C. Different time-points aliquots were received in 5× sample buffer and subjected to SDS-PAGE on 12% polyacrylamide gels. To test phosphatase activity, purified GST-DesR was phosphorylated with DesKC-P in reaction buffer, as previously described (Albanesi *et al*., 2004). GST-DesR~P was then re-purified with standard GST affinity chromatography and incubated with DesK or $DesK_{STA}$ at equimolar concentrations. Different time-points aliquots were withdrawn and received in 5× sample buffer. The reactions were analyzed by 12% SDS-PAGE. In all cases, the gels were dried and exposed for autoradiography. Bands corresponding to phosphorylated proteins were quantified by densitometry using the ImageJ software (National Institutes of Health. Whasington DC. U.S.A.). As the amount of protein integrated into the liposomes varies among different preparations, for comparative purposes, the activities were expressed as arbitrary units of phosphorylated protein per μg of WT DesK or $DesK_{STA}$ used, as indicated in the Figures corresponding to each assay.

Computational modeling and simulations

Systems were built by combining manual and scripting operations in PyMOL, VMD and NAMD, based on X-ray structures of DesKC H188V in PDB ID 3EHJ and H188E in 3GIE and considering the sequence-based topology predictions. Amino acids were added toward the N-terminus of each helix in each model following the corresponding amino acid sequence and considering the geometry predicted by the Coiled-coil Crick Parameterization tool (Crick, 1953b; Grigoryan and Degrado, 2011). Every turn of both helices, the growing segments were brought together through restrained minimization steps employing AMBER99SB (Hornak *et al*., 2006) descriptions of the protein in implicit solvent. The final models were minimized in implicit solvent with secondary structure restraints. Next, by employing the CHARMM-GUI (Jo *et al*., 2007; 2008) server, each of the three protein models was embedded in a DOPC or DEPC membrane as predicted by OPM (Lomize *et al*., 2006a,b) and hydrated with explicit water plus K^+ and Cl^- ions to 0.15 M concentration. Also inside CHARMM-GUI, the resulting systems were parameterized using CHARMM27 parameters for the protein, CHARMM36 parameters for lipids and a TIP3P (Jorgensen *et al*., 1983) model for water. The protocol provided by the CHARMM-GUI server was used in the NAMD program to equilibrate the systems up to 303.15 K and 1 atm. Production simulations were then carried out with NAMD too, using 2 fs time steps for integration and a cut-off at 12 Å for non-bonded interactions with a switching function from 10 to 12 Å and particle-mesh Ewald treatment of electrostatics with a grid spacing of 1 Å.

For modeling MS-DesK in the phosphatase form, the 2-HCC observed for DesKC in PDB ID 3EHJ was extended following the sequence of the minimal sensor and canonical

coiled coil parameters, as done for TM5-DesKC. This model relaxes in DOPC and DEPC membranes as described under *Results*.

Upon modeling MS-DesK in the kinase state, we first point out that the starting structure (DesKC in the autokinase-competent state, PDB ID 3GIE) reveals no canonical 2-HCC extending toward the membrane. Indeed, if its 4-HB is aligned to that of the phosphatase form, the helices are found to diverge toward the N-terminal side of the phosphorylatable His188 drifting away from each other (Fig. S9) (Albanesi *et al*., 2009). This separation is accompanied by their gradual rotation around their own axes relative to the structure of the phosphatase form, such that the first residues resolved in the X-ray structures (around residue 156–165 of MS-DesK's sequence in Fig. S10) are rotated by 70–90° in the kinase form relative to the phosphatase form (this is evidenced in Fig. S10 by rendering as sticks the charged residues of that segment, which are well exposed in the phosphatase form but brought together in the kinase form) (Albanesi *et al*., 2009). These motions are consistent with current proposals explaining how scissoring and helix tilting are coupled with rotational shifts during HK sensing (Lemmin *et al*., 2013; Molnar *et al*., 2014). By comparing the two DesKC structures, the helical rotations bring the side-chains of polar and charged residues into the interior of the coiled coil in the kinase form, opening it up by separating both helices (Fig. 6A, Figs S6 and S10) (Albanesi *et al*., 2009). However, the two helices should pair back in the transmembrane portion so as to 'zip' their polar residues by contacting each other and hide them from the hydrophobic membrane portion, a key point stemming intuitively from physicochemical principles but supported by a recent large-scale analysis of soluble and transmembrane helix–helix interactions (Deber and Ng, 2015; Zhang *et al*., 2015). Such a model turns out to require stretched, nearly parallel helices, instead of a coiled coil arrangement (Fig. S6B and D), and experiences asymmetric distortions during relaxation, all of these observations better described under *Results*.

Acknowledgements

This work was supported by grants from Consejo Nacional de Investigaciones Científicas y Técnicas (CONICET) and Agencia Nacional de Promoción Científica y Tecnológica (FONCYT PICT 2010-2613). L.A.A. thanks EMBO and the Marie Curie Actions for a postdoctoral fellowship. Parts of this work were done using computational resources from PRACE awarded to L.A.A., T.L. and M.D.P. M.D.P. is funded by the Swiss National Science Foundation. E.S. and Y.T.S. are fellows and D.d.M. and D.A. are Career Investigators of CONICET.

Conflict of interest

The authors declare no conflict of interest.

References

Aguilar, P.S., Lopez, P., and de Mendoza, D. (1999) Transcriptional control of the low-temperature-inducible des gene, encoding the delta5 desaturase of *Bacillus subtilis*. *J Bacteriol* **181:** 7028–7033.

Aguilar, P.S., Hernandez-Arriaga, A.M., Cybulski, L.E., Erazo, A.C., and de Mendoza, D. (2001) Molecular basis of thermosensing: a two-component signal transduction thermometer in *Bacillus subtilis*. *EMBO J* **20:** 1681–1691.

Albanesi, D., Mansilla, M.C., and de Mendoza, D. (2004) The membrane fluidity sensor DesK of *Bacillus subtilis* controls the signal decay of its cognate response regulator. *J Bacteriol* **186:** 2655–2663.

Albanesi, D., Martin, M., Trajtenberg, F., Mansilla, M.C., Haouz, A., Alzari, P.M., *et al*. (2009) Structural plasticity and catalysis regulation of a thermosensor histidine kinase. *Proc Natl Acad Sci USA* **106:** 16185–16190.

Altabe, S.G., Aguilar, P., Caballero, G.M., and de Mendoza, D. (2003) The *Bacillus subtilis* acyl lipid desaturase is a delta5 desaturase. *J Bacteriol* **185:** 3228–3231.

Anantharaman, V., Balaji, S., and Aravind, L. (2006) The signaling helix: a common functional theme in diverse signaling proteins. *Biol Direct* **25:** 1–16.

Bhate, M.P., Molnar, K.S., Goulian, M., and DeGrado, W.F. (2015) Signal transduction in histidine kinases: insights from new structures. *Structure* **23:** 981–994.

Blicher, A., Wodzinska, K., Fidorra, M., Winterhalter, M., and Heimburg, T. (2009) The temperature dependence of lipid membrane permeability, its quantized nature, and the influence of anesthetics. *Biophys J* **96:** 4581–4591.

Casino, P., Miguel-Romero, L., and Marina, A. (2014) Visualizing autophosphorylation in histidine kinases. *Nat Commun* **5:** 3258. doi:10.1038/ncomms4258

Crick, F. (1953a) The packing of alpha-helices: simple coiled-coils. *Acta Cryst* **6:** 689–697.

Crick, F.H. (1953b) The fourier transform of a coiled coil. *Acta Cryst* **6:** 685–689.

Cybulski, L.E., Albanesi, D., Mansilla, M.C., Altabe, S., Aguilar, P.S., and de Mendoza, D. (2002) Mechanism of membrane fluidity optimization: isothermal control of the *Bacillus subtilis* acyl-lipid desaturase. *Mol Microbiol* **45:** 1379–1388.

Cybulski, L.E., del Solar, G., Craig, P.O., Espinosa, M., and de Mendoza, D. (2004) *Bacillus subtilis* DesR functions as a phosphorylation-activated switch to control membrane lipid fluidity. *J Biol Chem* **279:** 39340–39347.

Cybulski, L.E., Martin, M., Mansilla, M.C., Fernandez, A., and de Mendoza, D. (2010) Membrane thickness cue for cold sensing in a bacterium. *Curr Biol* **20:** 1539–1544.

Cybulski, L.E., Ballering, J., Moussatova, A., Inda, M.E., Vazquez, D.B., Wassenaar, T.A., *et al*. (2015) Activation of the bacterial thermosensor DesK involves a serine zipper dimerization motif that is modulated by bilayer thickness. *Proc Natl Acad Sci USA* **112:** 6353–6358.

Dago, A.E., Schug, A., Procaccini, A., Hoch, J.A., Weigt, M., and Szurmant, H. (2012) Structural basis of histidine kinase autophosphorylation deduced by integrating genomics, molecular dynamics, and mutagenesis. *Proc Natl Acad Sci USA* **109:** E1733–E1742.

Deber, C.M., and Ng, D.P. (2015) Helix-helix interactions: is the medium the message? *Structure* **23:** 437–438.

Diensthuber, R.P., Bommer, M., Gleichmann, T., and Moglich, A. (2013) Full-length structure of a sensor histidine kinase pinpoints coaxial coiled coils as signal transducers and modulators. *Structure* **21:** 1127–1136.

Finn, R.D., Bateman, A., Clements, J., Coggill, P., Eberhardt, R.Y., Eddy, S.R., *et al*. (2014) Pfam: the protein families database. *Nucleic Acids Res* **42:** D222–D230.

Grigoryan, G., and Degrado, W.F. (2011) Probing designability via a generalized model of helical bundle geometry. *J Mol Biol* **405:** 1079–1100.

Grigoryan, G., and Keating, A.E. (2008) Structural specificity in coiled-coil interactions. *Curr Opin Struct Biol* **18:** 477–483.

Harwood, C.R., and Cuttings, S.M. (1990) *Molecular Biological Methods for Bacillus*. Chichester, UK: John Wiley & Sons.

Ho, S.N., Hunt, H.D., Horton, R.M., Pullen, J.K., and Pease, L.R. (1989) Site-directed mutagenesis by overlap extension using the polymerase chain reaction. *Gene* **77:** 51–59.

Hornak, V., Abel, R., Okur, A., Strockbine, B., Roitberg, A., and Simmerling, C. (2006) Comparison of multiple Amber force fields and development of improved protein backbone parameters. *Proteins* **65:** 712–725.

Inda, M.E., Vandenbranden, M., Fernandez, A., de Mendoza, D., Ruysschaert, J.M., and Cybulski, L.E. (2014) A lipid-mediated conformational switch modulates the thermosensing activity of DesK. *Proc Natl Acad Sci USA* **111:** 3579–3584.

Jambeck, J.P., and Lyubartsev, A.P. (2012) An extension and further validation of an all-atomistic force field for biological membranes. *J Chem Theory Comput* **8:** 2938–2948.

Jo, S., Kim, T., and Im, W. (2007). Automated builder and database of protein/membrane complexes for molecular dynamics simulations. *PLoS ONE* **2:** e880.

Jo, S., Kim, T., Iyer, V.G., and Im, W. (2008) CHARMM-GUI: a web-based graphical user interface for CHARMM. *J Comput Chem* **29:** 1859–1865.

Johansson, P., and Hederstedt, L. (1999) Organization of genes for tetrapyrrole biosynthesis in gram-positive bacteria. *Microbiology* **145** (Part 3): 529–538.

Jorgensen, W.L., Chandrasekhar, J., Madura, J.D., Impey, R.W., and Klein, M.L. (1983) Comparison of simple potential functions for simulating liquid water. *J Chem Phys* **79:** 926–935.

Kucerka, N., Liu, Y., Chu, N., Petrache, H.I., Tristram-Nagle, S., and Nagle, J.F. (2005) Structure of fully hydrated fluid phase DMPC and DLPC lipid bilayers using X-ray scattering from oriented multilamellar arrays and from unilamellar vesicles. *Biophys J* **88:** 2626–2637.

Lee, A.G. (2003) Lipid-protein interactions in biological membranes: a structural perspective. *Biochim Biophys Acta* **1612:** 1–40.

Lee, A.G. (2004) How lipids affect the activities of integral membrane proteins. *Biochim Biophys Acta* **1666:** 62–87.

Lee, A.G. (2011) Biological membranes: the importance of molecular detail. *Trends Biochem Sci* **36:** 493–500.

Lemmin, T., Soto, C.S., Clinthorne, G., DeGrado, W.F., and Dal Peraro, M. (2013) Assembly of the transmembrane domain of *E. coli* PhoQ histidine kinase: implications for signal transduction from molecular simulations. *PLoS Comput Biol* **9:** e1002878.

Leonenko, Z.V., Finot, E., Ma, H., Dahms, T.E., and Cramb, D.T. (2004) Investigation of temperature-induced phase transitions in DOPC and DPPC phospholipid bilayers using temperature-controlled scanning force microscopy. *Biophys J* **86:** 3783–3793.

Liu, J., Yang, J., Wen, J., Yang, Y., Wei, X., Zhang, X., and Wang, Y.P. (2014) Mutational analysis of dimeric linkers in peri- and cytoplasmic domains of histidine kinase DctB reveals their functional roles in signal transduction. *Open Biol* **4:** 140023. doi:10.1098/rsob.140023

Lomize, A.L., Pogozheva, I.D., Lomize, M.A., and Mosberg, H.I. (2006a) Positioning of proteins in membranes: a computational approach. *Protein Sci* **15:** 1318–1333.

Lomize, M.A., Lomize, A.L., Pogozheva, I.D., and Mosberg, H.I. (2006b) OPM: orientations of proteins in membranes database. *Bioinformatics* **22:** 623–625.

Lupas, A. (1996) Prediction and analysis of coiled-coil structures. *Methods Enzymol* **266:** 513–525.

Lupas, A., Van Dyke, M., and Stock, J. (1991) Predicting coiled coils from protein sequences. *Science* **252:** 1162–1164.

Mansilla, M.C., and de Mendoza, D. (1997) L-cysteine biosynthesis in *Bacillus subtilis*: identification, sequencing, and functional characterization of the gene coding for phosphoadenylylsulfate sulfotransferase. *J Bacteriol* **179:** 976–981.

Marina, A., Waldburger, C.D., and Hendrickson, W.A. (2005) Structure of the entire cytoplasmic portion of a sensor histidine-kinase protein. *EMBO J* **24:** 4247–4259.

Martin, M., and de Mendoza, D. (2013) Regulation of *Bacillus subtilis* DesK thermosensor by lipids. *Biochem J* **451:** 269–275.

Martin, M., Albanesi, D., Alzari, P.M., and de Mendoza, D. (2009) Functional in vitro assembly of the integral membrane bacterial thermosensor DesK. *Protein Expr Purif* **66:** 39–45.

Mathai, J.C., Tristram-Nagle, S., Nagle, J.F., and Zeidel, M.L. (2008) Structural determinants of water permeability through the lipid membrane. *J Gen Physiol* **131:** 69–76.

Mechaly, A.E., Sassoon, N., Betton, J.M., and Alzari, P.M. (2014) Segmental helical motions and dynamical asymmetry modulate histidine kinase autophosphorylation. *PLoS Biol* **12:** e1001776.

de Mendoza, D. (2014) Temperature sensing by membranes. *Annu Rev Microbiol* **68:** 101–116.

Miller, J.H. (1972) *Experiments in Molecular Genetics*. Cold Spring Harbor, NY: Cold Spring Harbor Laboratory.

Moglich, A., Ayers, R.A., and Moffat, K. (2009) Design and signaling mechanism of light-regulated histidine kinases. *J Mol Biol* **385:** 1433–1444.

Molnar, K.S., Bonomi, M., Pellarin, R., Clinthorne, G.D., Gonzalez, G., Goldberg, S.D., *et al*. (2014) Cys-scanning disulfide crosslinking and bayesian modeling probe the transmembrane signaling mechanism of the histidine kinase, PhoQ. *Structure* **22:** 1239–1251.

Muhle-Goll, C., Hoffmann, S., Afonin, S., Grage, S.L., Polyansky, A.A., Windisch, D., *et al*. (2012) Hydrophobic matching controls the tilt and stability of the dimeric platelet-derived growth factor receptor (PDGFR) beta transmembrane segment. *J Biol Chem* **287:** 26178–26186.

Pan, J., Tristram-Nagle, S., Kucerka, N., and Nagle, J.F. (2008) Temperature dependence of structure, bending rigidity, and bilayer interactions of dioleoylphosphatidylcholine bilayers. *Biophys J* **94:** 117–124.

Perego, M. (1993) Integrational vectors for genetic maniou-

lation in *Bacillus subtilis*. In Bacillus Subtilis *and Other Gram-positive Bacteria: Biochemistry, Physiology, and Molecular Genetics*. Sonenshein, A.L., Hoch, J.A., and Losick, R. (eds). Washington, DC: American Society for Microbiology, pp. 615–624.

Porrini, L., Cybulski, L.E., Altabe, S.G., Mansilla, M.C., and de Mendoza, D. (2014) Cerulenin inhibits unsaturated fatty acids synthesis in *Bacillus subtilis* by modifying the input signal of DesK thermosensor. *Microbiologyopen* **3:** 213–224.

Sambrook, J., Fritsch, E.F., and Maniatis, T. (1989) *Molecular Cloning: A Laboratory Manual*. New York: Cold Spring Harbor Laboratory, Cold Spring Harbor.

Singh, M., Berger, B., Kim, P.S., Berger, J.M., and Cochran, A.G. (1998) Computational learning reveals coiled coil-like motifs in histidine kinase linker domains. *Proc Natl Acad Sci USA* **95:** 2738–2743.

Spizizen, J. (1958) Transformation of biochemically deficient strains of *Bacillus subtilis* by deoxyribonucleate. *Proc Natl Acad Sci USA* **44:** 1072–1078.

Szekely, P., Dvir, T., Asor, R., Resh, R., Steiner, A., Szekely, O., *et al*. (2011) Effect of temperature on the structure of charged membranes. *J Phys Chem B* **115:** 14501–14506.

Trajtenberg, F., Grana, M., Ruetalo, N., Botti, H., and Buschiazzo, A. (2010) Structural and enzymatic insights into the ATP binding and autophosphorylation mechanism of a sensor histidine kinase. *J Biol Chem* **285:** 24892–24903.

Trajtenberg, F., Albanesi, D., Ruetalo, N., Botti, H., Mechaly, A.E., Nieves, M., *et al*. (2014) Allosteric activation of bacterial response regulators: the role of the cognate histidine kinase beyond phosphorylation. *MBio* **5:** e02105.

Wang, C., Sang, J., Wang, J., Su, M., Downey, J.S., Wu, Q., *et al*. (2013) Mechanistic insights revealed by the crystal structure of a histidine kinase with signal transducer and sensor domains. *PLoS Biol* **11:** e1001493.

Xu, Q., Kim, M., Ho, K.W., Lachowicz, P., Fanucci, G.E., and Cafiso, D.S. (2008) Membrane hydrocarbon thickness modulates the dynamics of a membrane transport protein. *Biophys J* **95:** 2849–2858.

Zhang, S.Q., Kulp, D.W., Schramm, C.A., Mravic, M., Samish, I., and DeGrado, W.F. (2015) The membrane- and soluble-protein helix-helix interactome: similar geometry via different interactions. *Structure* **23:** 527–541.

Zhang, Y.M., and Rock, C.O. (2008) Membrane lipid homeostasis in bacteria. *Nat Rev Microbiol* **6:** 222–233.

Supporting information

Additional supporting information may be found in the online version of this article at the publisher's web-site.